Int J Adv Manuf Technol (2017) 91:3371–3384
DOI 10.1007/s00170-017-9999-4

ORIGINAL ARTICLE

Rapid prediction of longitudinal curvature obtained by flexibly reconfigurable roll forming using response surface methodology

Ji-Woo Park[1] · **Junseok Yoon**[1] · **Kyounghoon Lee**[2] · **Jeong Kim**[1] · **Beom-Soo Kang**[2]

Received: 9 October 2016 / Accepted: 3 January 2017 / Published online: 22 January 2017

Abstract Flexibly reconfigurable roll forming (FRRF) is a sheet-forming technology that can be used to produce multi-curvature surfaces by controlling the longitudinal strain distribution. In FRRF, the shape of the formed surface is determined by the curvature of the reconfigurable rollers and the gaps between the rollers. Because FRRF technology is still under development, a simulation model of the physical forming process is conveniently used to investigate the effects of the input parameters. To facilitate the investigation in the present study, the response surface methodology is used to develop a model for predicting the curvature produced in a longitudinal blank. The input parameters are the sheet compression ratio, the curvature radius in the transverse direction, and the initial blank width. Samples are generated using a three-level three-factor full-factorial design, and each convex and saddle curvature is represented by a quadratic regression model with two-factor interactions. The fitted polynomial equations are verified numerically by the R-squared values and root mean square errors and graphically by residual plots. To assess the reliability of the sample data, experiments are performed using pre-FRRF equipment. The proposed analytical procedure is confirmed to be reasonable, and a statistical formula for estimating the longitudinal curvature produced by the FRRF process is established.

Keywords Flexibly reconfigurable roll forming · Response surface methodology · Regression analysis · Experiments and numerical simulations

✉ Beom-Soo Kang
bskang@pusan.ac.kr

Ji-Woo Park
lgslgsl@naver.com

Junseok Yoon
hamjang21c@gmail.com

Kyounghoon Lee
aeronova@pusan.ac.kr

Jeong Kim
greatkj@pusan.ac.kr

[1] Department of Aerospace Engineering, Pusan National University, Busan 46241, South Korea

[2] ERC-ITAF, Pusan National University, Busan 46241, South Korea

1 Introduction

Flexible forming offers an alternative to labour-intensive production methods. The technique can be used to simultaneously improve productivity and quality. Multi-point dieless forming (MDF) is a representative example of flexible forming and has been actively studied. Heo et al. showed that the main advantage of MDF was its flexibility, which enables the implementation of various shapes of the punches using a single apparatus, thereby reducing the cost of the punch set [1]. However, the technique has some disadvantages, which include faulty forming characterised by wrinkling and dimpling. These problems were investigated by Quan et al. [2]. Another disadvantage of the technique is the limitation of the forming area by the dimensions of the apparatus.

Wang et al. recently proposed a new concept of flexible forming referred to as flexible rolling [3]. Flexible rolling can be used to fabricate a multi-curvature shape using flexible rollers. As Yoon et al. noted, the desired roller curvature in the case of flexibly reconfigurable roll forming (FRRF) can be achieved by appropriate adjustment of the curvature punches [4]. FRRF utilises continuous rollers, and this eliminates the dimpling problem. Furthermore, the forming size in the rolling

direction is unlimited and the process is more economical compared to MDF. FRRF is, however, still under development, and it is very difficult to predict the forming results. The development of a method for predicting the forming results would constitute an essential progress toward actual application of the technology. It is actually possible to predict the shape of the objective surface by FEM simulation before performing a real forming experiment. However, the procedure requires the simulation of every single case and this could be time-consuming. The response surface methodology is used to remedy this disadvantage. In addition, regression analysis is a statistical method that can be used to estimate an output of interest to obtain a polynomial equation model of the output as a function of the inputs. Regression analysis can thus be used to obtain a statistical formula for correlating the input forming parameters with the target curvatures. Myers et al. published a book about the response surface methodology [5], which is widely used in the materials and manufacturing industries. Ganjigatti et al. also used regression analysis to investigate the input-output relationship for metal inert gas welding [6]. Furthermore, Çaydaş and Hasçalık posited that the waterjet pressure significantly affected the surface roughness [7]. In the present study, a regression model and an artificial neural network were employed. Bashah et al. investigated the use of a regression model to predict the effect of springback on white-stamped automotive body parts [8]. The considered regression analysis model was developed for flexible forming. Seo et al. also used regression analysis and a neural network model to investigate the shape error of flexible stretch forming [9].

In the present study, the curvature radius in the longitudinal direction is considered as the dependent variable (that is, the output parameter) of the regression analysis, with the independent variables (that is, the input parameters) comprising the compression ratio of the sheet, curvature radius in the transverse direction, and width of the original blank. The response surface methodology is used to predict the results of the FRRF process by regression analysis.

2 Basic concept of FRRF

The basic principle of FRRF is strain control. The strain difference arising from compression variation between the centre line and the edge line during the roll forming process produces a length difference between the centre and the edge of the blank, resulting in the formation of a curvature. The FRRF PCT patent was submitted by Kang and Yoon [10]. The schematic illustration of the FRRF process shown in Fig. 1 is included in the patent of Kang and Yoon. The reconfigurable rollers, which can be flexibly bent, are arranged on top of each other. The blank is inserted between the upper and down rollers, and the upper roller moves downward to compress it.

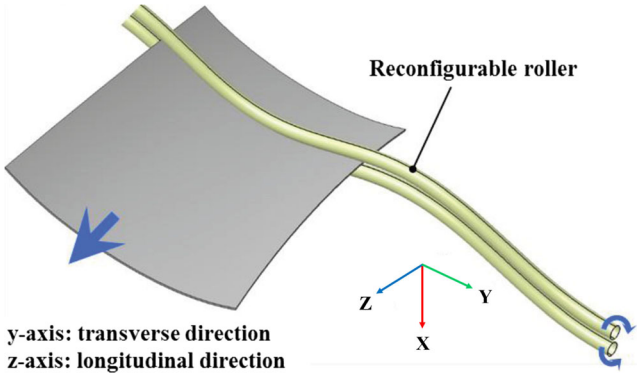

Fig. 1 Schematic illustration of the FRRF process

After the compression, the two rollers are rotated to roll the formed sheet. The compression is the primary means of forming a longitudinal curvature based on the difference between the strain distributions. For instance, when the strain at the centre of the sheet is higher than that at the tip, the formed longitudinal curvature would have a convex shape. The reverse case produces a longitudinal curvature with a saddle shape. The translocation of the curvature adjustment rods is used to vary the curvature of the reconfigurable rollers. The schematic diagram of the flexible rollers and curvature adjustment rods shown in Fig. 2 is also included in the patent of Kang and Yoon.

The position of each roller is determined by the objective curvature radius in the transverse direction, the compressive strain difference between the centre and tip of the blank, and the width (length in the transverse direction) of the original blank. The basic position of each roller is first set based on the objective curvature of the sheet in the transverse direction. The final position of each roller is then calculated based on

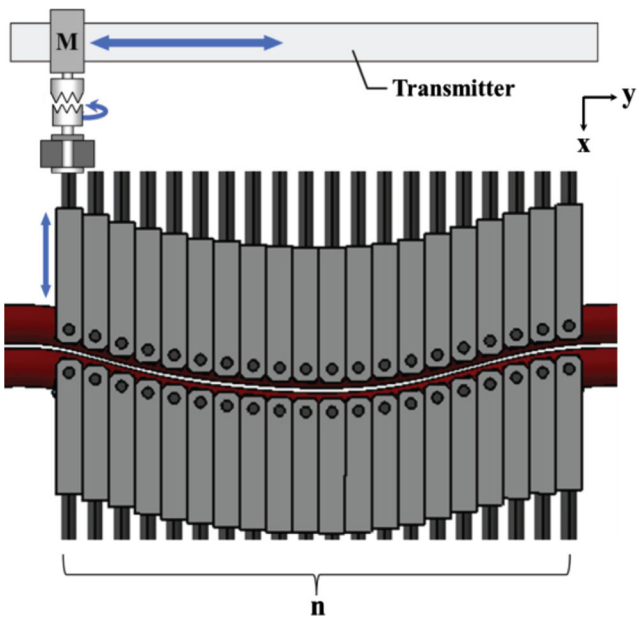

Fig. 2 Schematic of reconfigurable roller and curvature adjustment rods

the compressive strain. Generally, the compressive strain is limited to 10% of the initial blank thickness owing to the extreme difficulty of achieving higher strains. The ratio of the compression at the tip of the blank to that at the centre is used as the first main input parameters in the present study. This is required to determine the compression at each of the two points. The curvature radius in the transverse direction of the blank is used as the second input parameter, and the third is the width (length in the transverse direction) of the original blank. In other words, the geometrical curve of each roller is determined by the above three parameters, based on which the position of the roller is then calculated. The three parameters constitute the independent variables of the present regression analysis.

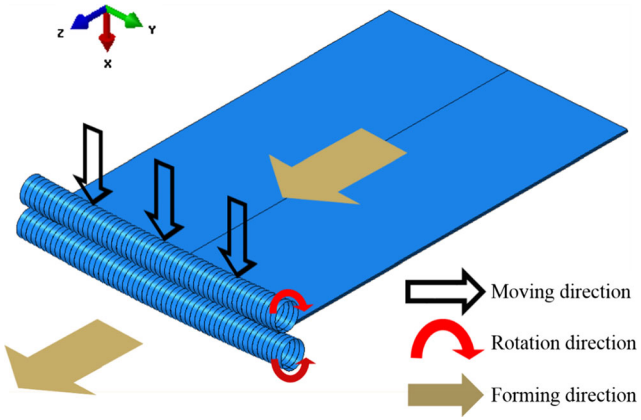

Fig. 3 FRRF simulation model

3 FE simulation

3.1 FE simulation model

The initial blank is an Al 2024-T3 sheet of thickness 1 mm. The physical properties of the material are as follows: Young's modulus = 73.1 GPa, Poisson's ratio = 0.33, and density = 2.78 g/cm^3. The Hollomon's n^{th} work hardening model ($\overline{\sigma} = K\overline{\varepsilon}^n$) is used to imitate the plastic behaviour of the material. The yield stress is 275 MPa, and the ultimate tensile stress is 430 MPa. Table 1 summarises the material properties of Al 2024-T3 that are used for the FE simulation.

The numerical simulations are performed using the FEM dynamic explicit solver of ABAQUS, a commercial numerical analysis software. In order to implement the reconfigurable roller, numerous rings are used as shown in Fig. 3. Each ring is arranged in the tangential direction of the curve which is calculated applying compression ratio. All the rings are modelled as discrete rigid shell elements (R3D4), and the blank is assumed to be a deformable eight-node linear brick element (C3D8R). To consider the variation in the thickness direction of the blank, four element layers are set in that direction. The number of elements varies with the size of the sheet, being about 21,000–33,000, and the friction coefficient is assumed to be 0.1. The numerical simulation comprises two steps. In the first step, which is the compression step, the flexible rollers are simulated by an array of multiple rings, each of diameter 20 mm and width 2 mm. The positions of the flexible rollers are set based on the objective shape, and the upper roller moves downward during a compression process. In the second step, which is the rotation step, the formed sheet is extruded by the rotation of all the rings at the same speed. The complete simulation model of the FRRF process is shown in Fig. 3. As depicted in the figure, there are two major boundary conditions, namely, compression down stroke and rotation of the rings.

Table 1 Material properties of Al 2024-T3

Material property		Value	Unit
Young's modulus		73.10	GPa
Poisson's ratio		0.33	–
Yield strength		275.00	MPa
Ultimate strength		430.00	MPa
Density		2.78	g/cm^3
Flow stress curve ($\overline{\sigma} = K\overline{\varepsilon}^n$)	K	690	MPa
	n	0.16	–

3.2 FE simulation cases

The regression analysis requires the selection of the dependent and independent variables. The dependent variable in the present study is the curvature radius in the longitudinal direction, and the independent variables are the ratio of the compression at the tip of the blank to that at the centre, the curvature radius of the original blank in the transverse direction, and the initial width of the blank. Each of the three independent variables is defined at three levels for a full factorial design. In other words, a three-factor three-level full-factorial design is employed. The levels of the design variables are given in Table 2. Because of the difficulty of compressing a thin sheet material by more than 10% of its thickness, the maximum compression is limited to 10%. In addition, considering that the objective shape is visualised as clearly requiring more than 5% compression, the minimum compression is fixed at 5%. The limits of the other design variables are selected based on the dimensions of the experimental apparatus currently in production.

Table 2 Levels of the design variables

	Level of factor		
Design variable (saddle shape)			
Compression ratio (tip/centre)	5/1	7/1	10/1
Curvature radius (mm)	500	700	1000
Width (mm)	100	125	150
Design variable (convex shape)			
Compression ratio (tip/centre)	1/5	1/7	1/10
Curvature radius (mm)	500	700	1000
Width (mm)	100	125	150

When the compression ratio exceeds 1.0, a saddle shape is formed, whereas a convex shape is formed when the compression ratio is less than 1.0. It is necessary to consider two cases of each shape. The statistical data for the saddle and convex shapes are given in Tables 3 and 4, respectively. A total of 54 simulations are performed.

3.3 Results of FE simulation

Figure 4 shows the simulation results for case 1, which has a saddle shape. To produce this shape, the compression at the tip should be higher than that at the centre. As can be observed from Fig. 4a, the maximum stress is about 345 MPa. Because the tip compression is higher than the central compression, the former area is subjected to a high stress. As in the stress distribution, the occurrence of high strain at the tip can be observed from Fig. 4b. Figure 5 shows the simulation results for case 28, which has a convex shape. As opposed to the saddle case, the compression at the tip in this case is less than that at the centre. The maximum stress, as can be observed from Fig. 5a, is about 358 MPa. In addition, as

Table 3 Statistical table for saddle shape

Number of case	Compression ratio X_1	Curvature radius of blank X_2 (mm)	Width of blank X_3 (mm)	Result (mm)
1	5.0	500	100	Y_1
2	5.0	500	125	Y_2
3	5.0	500	150	Y_3
4	5.0	700	100	Y_4
5	5.0	700	125	Y_5
6	5.0	700	150	Y_6
7	5.0	1000	100	Y_7
8	5.0	1000	125	Y_8
9	5.0	1000	150	Y_9
10	7.0	500	100	Y_{10}
11	7.0	500	125	Y_{11}
12	7.0	500	150	Y_{12}
13	7.0	700	100	Y_{13}
14	7.0	700	125	Y_{14}
15	7.0	700	150	Y_{15}
16	7.0	1000	100	Y_{16}
17	7.0	1000	125	Y_{17}
18	7.0	1000	150	Y_{18}
19	10.0	500	100	Y_{19}
20	10.0	500	125	Y_{20}
21	10.0	500	150	Y_{21}
22	10.0	700	100	Y_{22}
23	10.0	700	125	Y_{23}
24	10.0	700	150	Y_{24}
25	10.0	1000	100	Y_{25}
26	10.0	1000	125	Y_{26}
27	10.0	1000	150	Y_{27}

Table 4 Statistical table for convex shape

Number of case	Compression ratio X_1	Curvature radius of blank X_2 (mm)	Width of blank X_3 (mm)	Result (mm)
28	0.2	500	100	Y_{28}
29	0.2	500	125	Y_{29}
30	0.2	500	150	Y_{30}
31	0.2	700	100	Y_{31}
32	0.2	700	125	Y_{32}
33	0.2	700	150	Y_{33}
34	0.2	1000	100	Y_{34}
35	0.2	1000	125	Y_{35}
36	0.2	1000	150	Y_{36}
37	0.142857	500	100	Y_{37}
38	0.142857	500	125	Y_{38}
39	0.142857	500	150	Y_{39}
40	0.142857	700	100	Y_{40}
41	0.142857	700	125	Y_{41}
42	0.142857	700	150	Y_{42}
43	0.142857	1000	100	Y_{43}
44	0.142857	1000	125	Y_{44}
45	0.142857	1000	150	Y_{45}
46	0.1	500	100	Y_{46}
47	0.1	500	125	Y_{47}
48	0.1	500	150	Y_{48}
49	0.1	700	100	Y_{49}
50	0.1	700	125	Y_{50}
51	0.1	700	150	Y_{51}
52	0.1	1000	100	Y_{52}
53	0.1	1000	125	Y_{53}
54	0.1	1000	150	Y_{54}

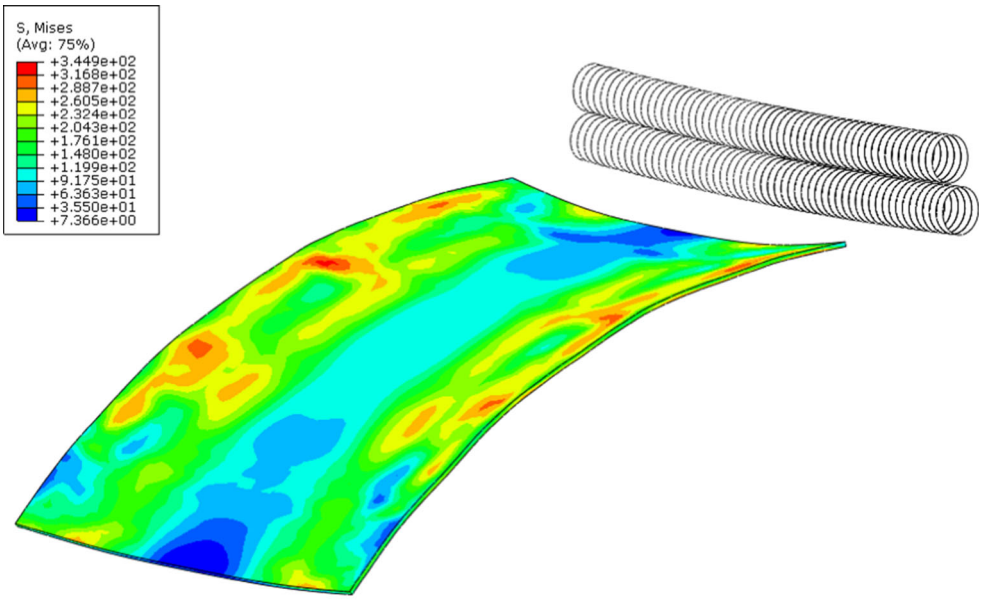

(a) Stress distribution

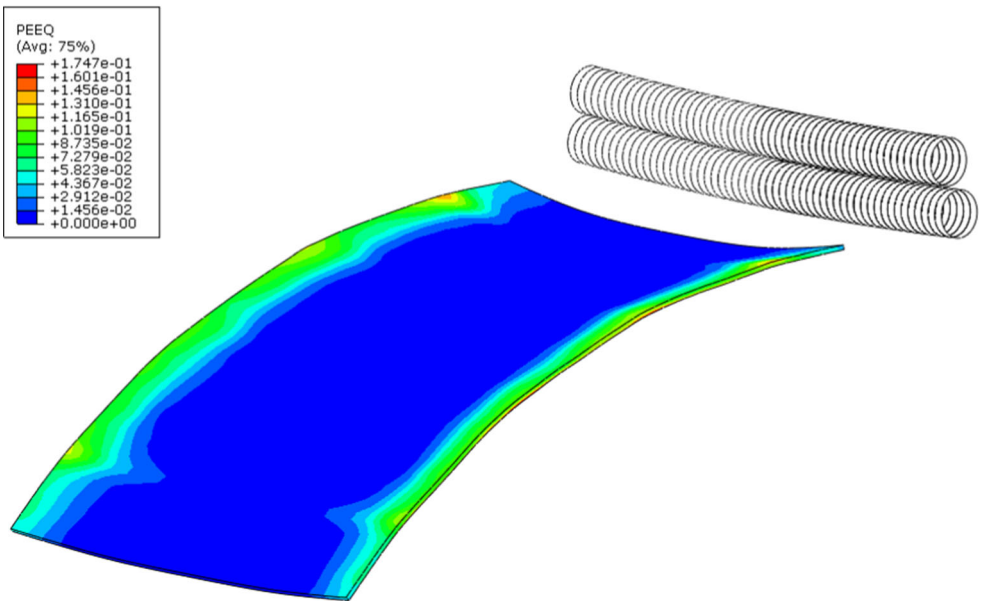

(b) Strain distribution

Fig. 4 Results of numerical simulation for saddle shape (stress and strain distributions)

opposed to the case of the saddle shape, the strain distribution is higher at the centre than at the tip (see Fig. 5b). The curvature in the longitudinal direction is the dependent variable and has to be determined. In the present simulations, the curvature is calculated using a three-point arc. Relative to the centre line, each point is used as the starting point, centre point, and end point. To facilitate understanding, Fig. 6 shows the curvature for the general case. The measured curvatures are presented in Table 5 with respect to the shape. These results are used as the sample data for the regression analysis.

4 Regression analysis

4.1 Regression analysis model

It is confirmed that the compression ratio of the sheet, the curvature radius of the original blank in the transverse direction, and the width of the original blank affect the dependent variable. The numbers of factors and levels are both three. To determine the appropriate regression model, it is necessary to investigate the main effects of the independent variables and the interactions

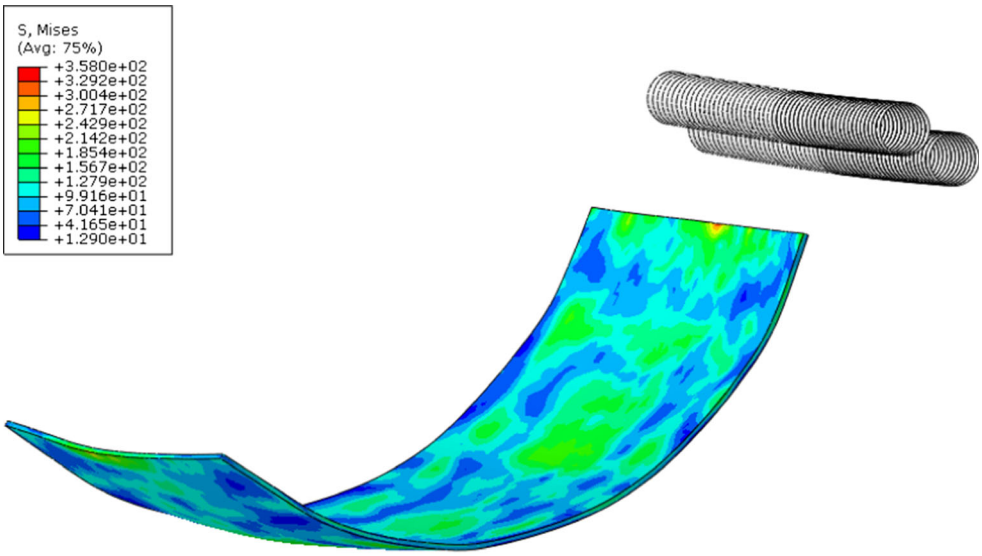

(a) Stress distribution

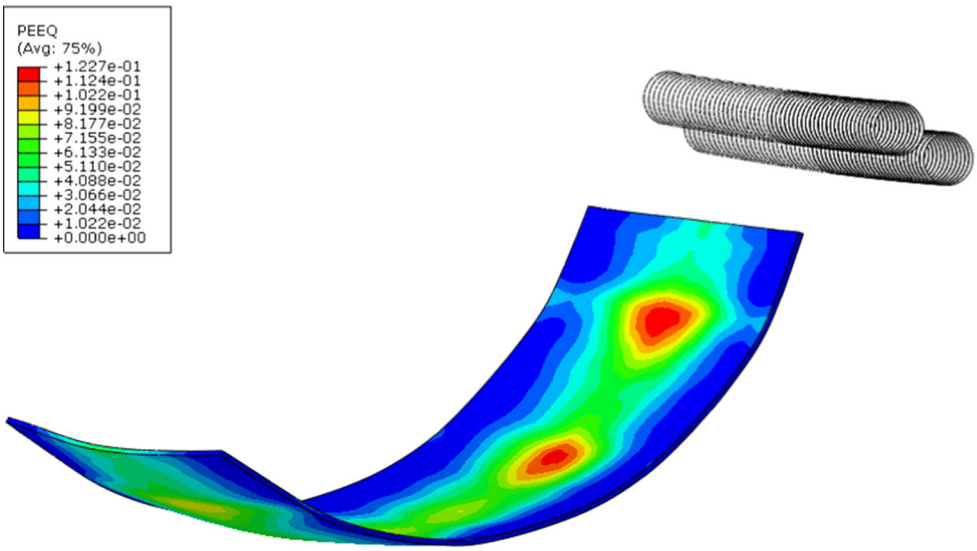

(b) Strain distribution

Fig. 5 Results of numerical simulation for convex shape (stress and strain distributions)

among them. The main effect of an independent variable is the mean change in the dependent variable produced by a variation of that particular independent variable. The interactions are the correlations among the different independent variables. The main effects and the interactions of the independent variables are determined using the MATLAB software. Figure 7 shows the main effects of the different design variables, where X_1 is the compression ratio, X_2 is the curvature radius of the original blank in the transverse direction, and X_3 is the width of the original blank. All the design variables have mildly quadratic effects on the dependent variable. Figure 8 shows the interactions among the design variables. Differences can be observed among the slopes of the interaction graphs, indicating different degrees of interactions among the design variables. The appropriate

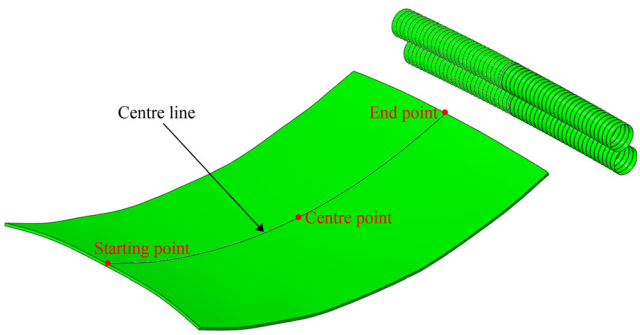

Fig. 6 Centre line of general model for numerical simulation

Table 5 Results of curvature measurement

Number of case (saddle)	Longitudinal curvature radius (mm)	Number of case (convex)	Longitudinal curvature radius (mm)
1	270.76	28	178.44
2	223.96	29	194.48
3	211.78	30	195.37
4	375.63	31	253.92
5	323.55	32	204.60
6	288.91	33	231.71
7	485.15	34	266.86
8	428.00	35	316.58
9	401.70	36	302.14
10	189.12	37	77.78
11	166.97	38	88.17
12	166.72	39	118.19
13	222.39	40	88.75
14	212.92	41	98.45
15	205.82	42	104.29
16	258.33	43	103.26
17	241.08	44	126.55
18	249.00	45	120.50
19	130.18	46	43.67
20	118.09	47	50.99
21	110.93	48	51.07
22	158.67	49	46.75
23	152.11	50	51.73
24	140.39	51	56.97
25	183.67	52	49.91
26	168.12	53	55.56
27	184.05	54	64.11

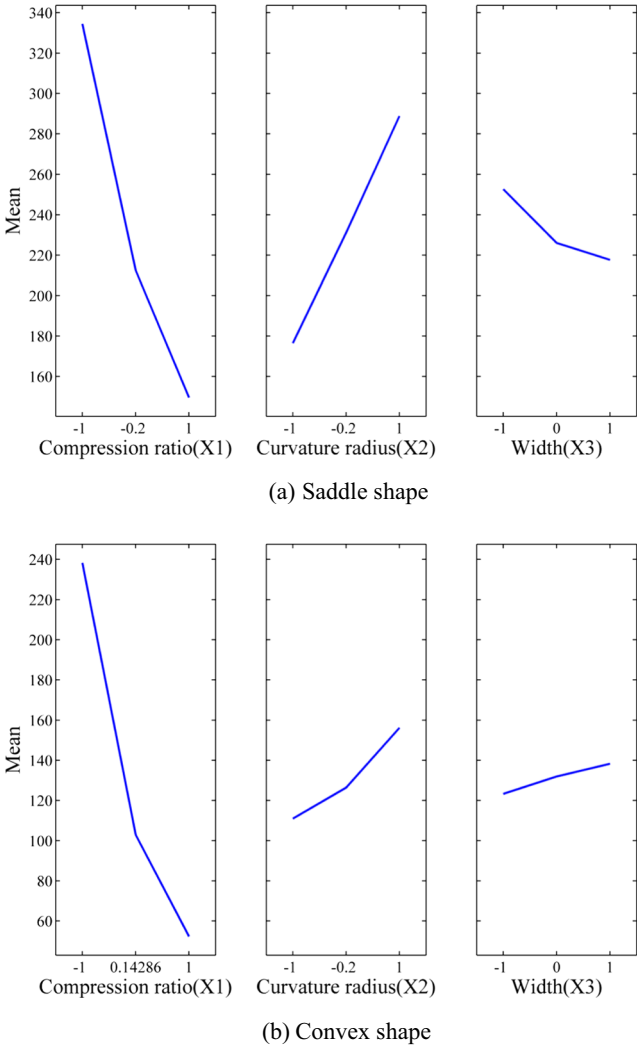

Fig. 7 Plots of main effects of design variables

regression analysis model that is used in this study is as follows:

$$y = \beta_0 + \beta_1 X_1 + \beta_{11} {X_1}^2 + \beta_2 X_2 + \beta_{22} {X_2}^2 + \beta_3 X_3 + \beta_{33} {X_3}^2 + \beta_{12} X_1 X_2 + \beta_{23} X_2 X_3 + \beta_{31} X_3 X_1 + E \quad (1)$$

where y is the dependent variable, x_i are the independent variables, β_i are the regression coefficients, and E is the error value. After the determination of the regression model, it is necessary to estimate the regression coefficients β_i from the data obtained by the simulations. Generally, the coefficients can be obtained by the method of least squares, which is one of the most widely used statistical estimation methods. The least squares method is used to calculate the regression coefficients in Eq. 1 such that the sum of the error E values is minimised. Hence, the function of the least squares method can be expressed as Eq. 2, which can be simplified in matrix form. This equation is cited by Myers et al. [5].

$$\mathrm{LSM} = \sum_{i=1}^{n} E^2 = E^T \cdot E = (\mathbf{y} - \mathbf{X}\boldsymbol{\beta})^T \cdot (\mathbf{y} - \mathbf{X}\boldsymbol{\beta}) \quad (2)$$

where E, $\mathbf{y}$, $\boldsymbol{\beta}$, and $\mathbf{X}$ are as follows:

$$E = \begin{bmatrix} E_1 \\ E_2 \\ \vdots \\ E_n \end{bmatrix}, \mathbf{y} = \begin{bmatrix} y_1 \\ y_2 \\ \vdots \\ y_n \end{bmatrix}, \boldsymbol{\beta} = \begin{bmatrix} \beta_1 \\ \beta_2 \\ \vdots \\ \beta_n \end{bmatrix}, \mathbf{X} = \begin{bmatrix} 1 & x_{11} & x_{21} & \cdots & x_{p1} \\ 1 & x_{12} & x_{22} & \cdots & x_{p2} \\ \vdots & \vdots & \vdots & \ddots & \vdots \\ 1 & x_{1n} & x_{2n} & \cdots & x_{pn} \end{bmatrix} \quad (3)$$

where n is the number of cases and p is the number of independent variables in each interaction.

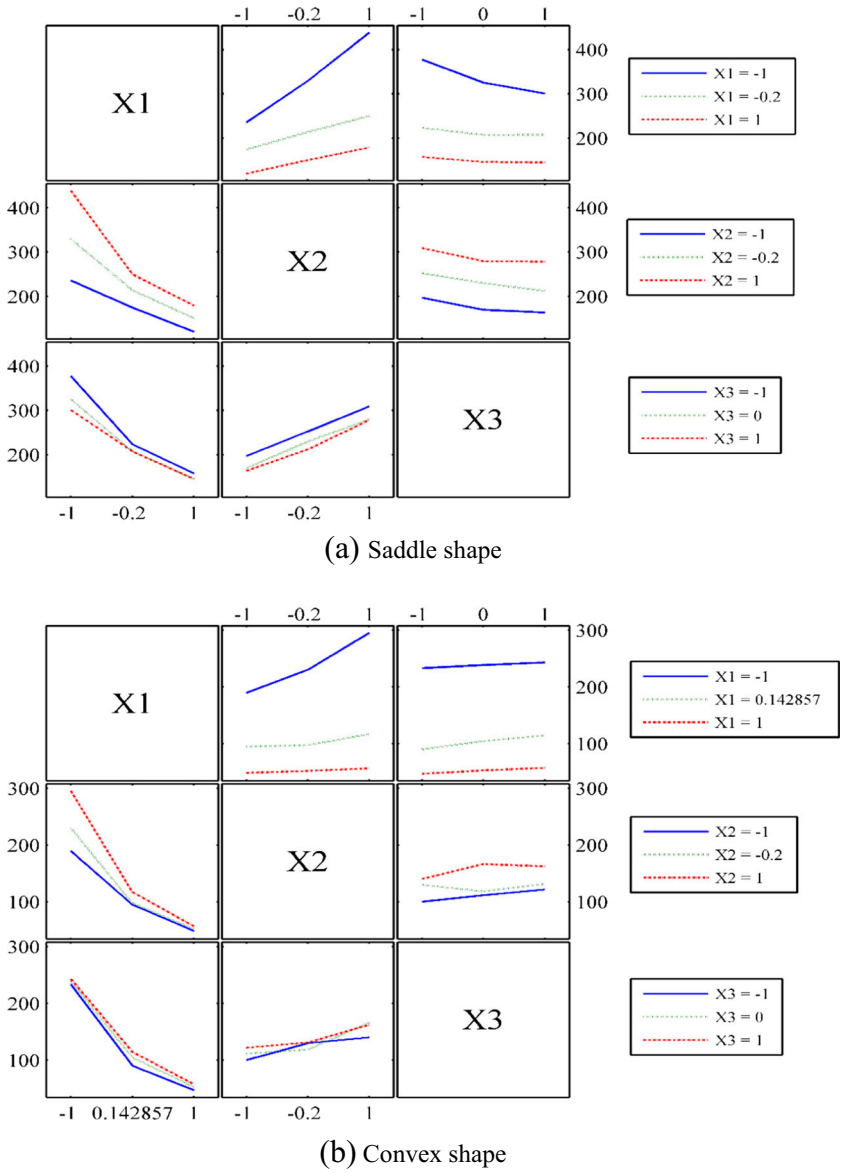

Fig. 8 Plots of the interactions of the design variables

Equation 3 is solved for the regression coefficients as follows:

$$\boldsymbol{\beta} = \left(\mathbf{X}^T \cdot \mathbf{X}\right)^{-1} \mathbf{X}^T \cdot \mathbf{y} \tag{4}$$

There are 10 unknown coefficients in the present study, and those estimated using Eq. 4 are presented in Table 6.

Table 6 Estimated regression coefficients

Regression coefficient (β_i)	Value (saddle shape)	Value (convex shape)
β_0	196.4367	116.0229
β_1	−94.6344	−94.6400
β_{11}	49.9766	29.7137
β_2	53.9111	23.8259
β_{22}	−10.1440	2.7678
β_3	−16.4237	7.5338
β_{33}	9.0889	−1.1406
β_{12}	−33.4917	−25.1499
β_{23}	0.9515	0.8446
β_{31}	14.8591	0.4839

4.2 Goodness-of-fit test of regression model

A fit test is used to verify the regression model. First, it is necessary to determine the coefficient of determination, namely, the R-squared value, which is the yardstick for evaluating the suitability of a regression model developed using actual data. In other words, the R-squared value is a measure of the

variability of y accounted for by the regression variables of a model. It is defined as follows:

$$R^2 = \frac{\mathrm{SSR}}{\mathrm{SST}} = 1 - \frac{\mathrm{SSE}}{\mathrm{SST}} \tag{5}$$

where $\mathrm{SSR} = \sum(\hat{y}_i - \bar{y})^2$, $\mathrm{SST} = \sum(y_i - \bar{y})^2$, and $\mathrm{SSE} = \sum(y_i - \hat{y}_i)^2$. *SSE* is the error sum of square, SST is the total sum of square, SSR is the regression sum of square, $\bar{y}$ is the average value of the data, y_i denotes the actual data values, and y_i denotes the estimated data values. The root mean square error (RMSE) is an intuitive and reasonable accuracy evaluation metric, while the normalised root mean square error (NRMSE) is used to evaluate the relative accuracy of the regression model using Eq. 6.

$$\mathrm{NRMSE} = \sqrt{\frac{\mathrm{SSE}}{n}} \cdot \frac{1}{(y_{\max} - y_{\min})} \tag{6}$$

In the case of the saddle shape, the R-squared value and NRMSE are determined to be 0.9724 and 0.0423, respectively, and the corresponding results for the case of the convex shape are 0.9791 and 0.0443, respectively. As can be observed, the R-squared values are nearly 1, which indicates that the regression model fitted the data well. In addition, the NRMSE values are almost 0, indicating very high accuracy of the regression model. The regression model can thus be considered appropriate.

It is also necessary to examine the precise difference between the actual data and the data estimated by the regression model. This difference is known as the error. Figure 9a, b shows the graphs of the observed curvature versus the predicted curvature, and Fig. 10a, b shows the differences between the original and estimated data, for the saddle and convex shapes, respectively. As can be observed from the figures, the trends of the estimations for both cases are similar. To evaluate the accuracy of the estimation model, the percentage errors are calculated. The maximum and minimum percentage errors for the saddle cases are determined to be about 18.8154 and 0.1201%, respectively. However, most of the percentage errors for the saddle cases are less than 10%, with the mean percentage error being

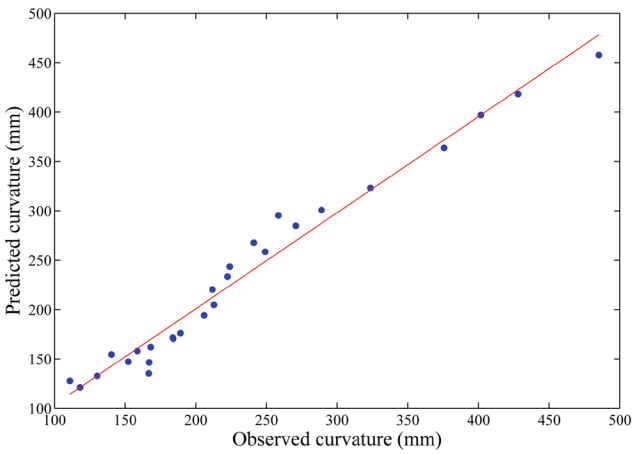

(a) Saddle shape

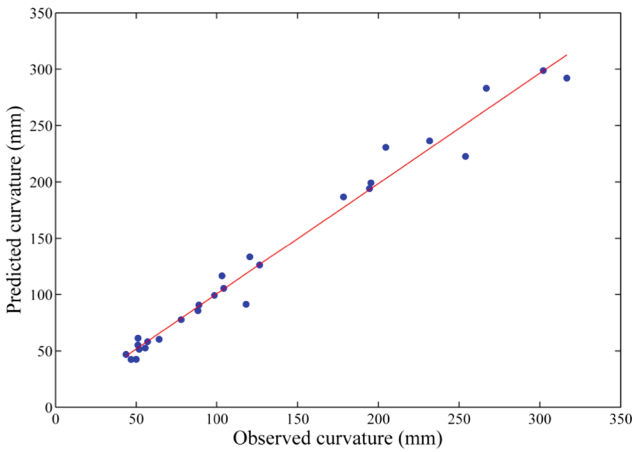

(b) Convex shape

Fig. 9 Graph of observed versus predicted curvature

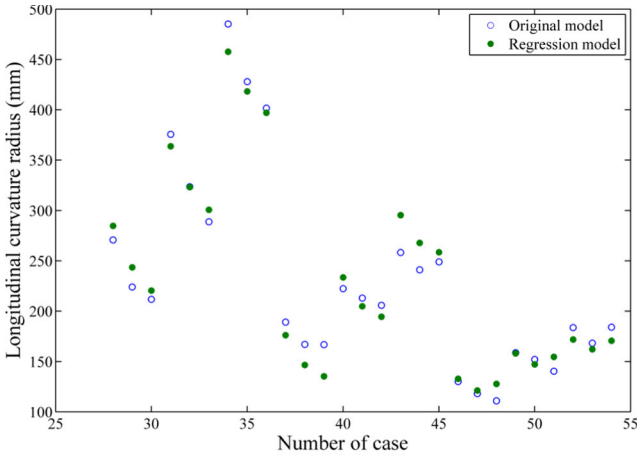

(a) Saddle shape

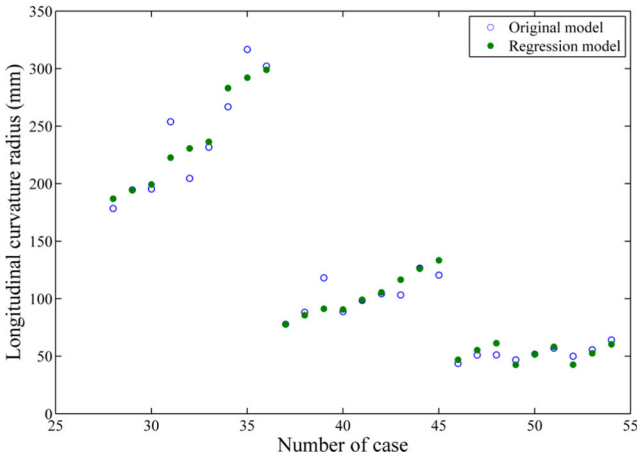

(b) Convex shape

Fig. 10 Difference between original and estimated data

6.1826%. The corresponding values for the convex cases are almost the same; the maximum and minimum percentage errors are respectively 22.7838 and 0.0448%, and the mean percentage error is 6.5103%. This confirms the suitability of the regression model and its usefulness for understanding the general trend of the FRRF process. The model can thus be used to predict the results of the process. Figure 11a, b shows the residual plots for the saddle and convex shapes, respectively. The observation of a definite pattern in a residual plot indicates that there are some missing variables in the regression model. However, no definite pattern is apparent in Fig. 11, indicating that there are no missing variables in the obtained regression model. The residual means are also examined, and the values for the saddle and convex shapes are determined to be respectively −2.477e−7 and 1.645e−15, which are almost 0. The results of the goodness-of-fit tests for both cases are summarised in Table 7.

One of the most important assumptions of the response surface methodology is that the error has a Gaussian distribution with zero mean, and this is also assumed in the application of the least square method. It is therefore necessary to examine the normality of the sample data. Figure 12 shows the normality plots. In the saddle case, almost all the sample data match the normal distribution. However, the normality plot for the convex case contains some discrepancies for high residual values. A frequency distribution histogram of some sample data is used to ascertain the normality of the

Table 7 Summary of results of goodness of fit tests

Summary of fit	Saddle shape	Convex shape
R-squared	0.9724	0.9791
Normalised root mean square error (NRMSE)	0.0423	0.0443
Maximum percent error	18.8154	22.7838
Minimum percent error	0.1201	0.0448
Mean percent error	6.1826	6.5103
Mean residual	−2.477e−7	1.645e−15
Variance of residual	6.7699	0.5483

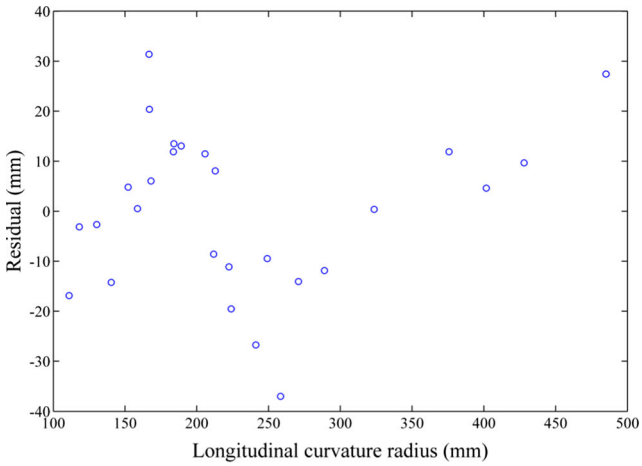

(a) Saddle shape

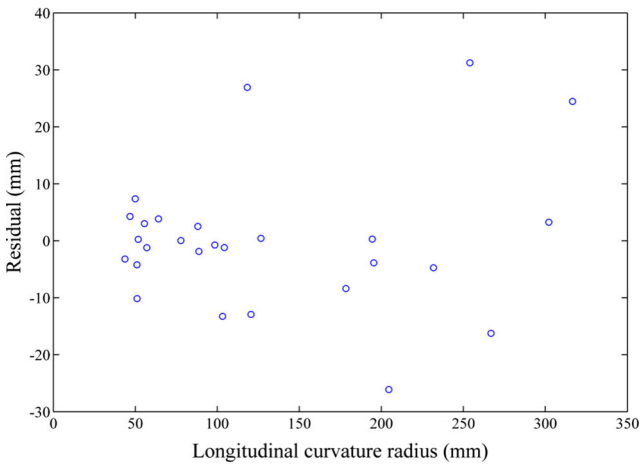

(b) Convex shape

Fig. 11 Plot of residual

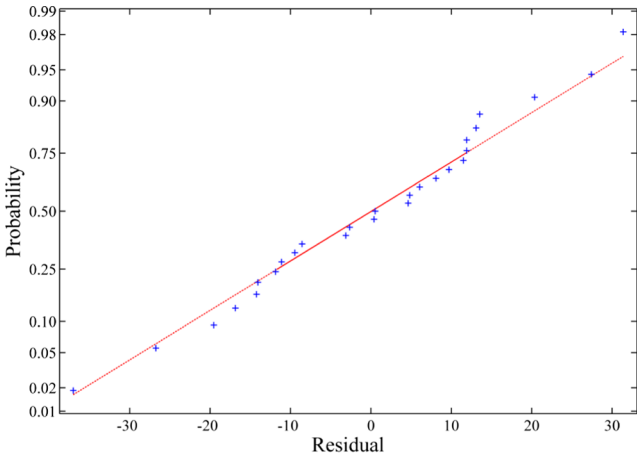

(a) Saddle shape

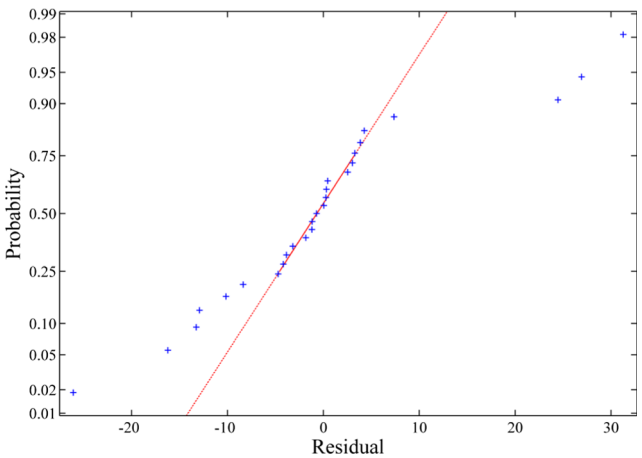

(b) Convex shape

Fig. 12 Normality plot

distributions. Figure 13a, b shows the histogram for each case. As can be observed, both graphs are bell-shaped, which indicates a normal distribution of the model results. The curve in Fig. 13a has a perfect bell shape, while that in Fig. 13b has a bell shape with long tails. This means that the tails of the error distribution for the convex shape are longer than those of a Gaussian distribution.

4.3 Random sample test

In Sect. 4.2, the suitability of the regression model was confirmed. However, to ascertain the applicability of the model to other cases, a random sample test is also conducted. Random sample data with the same limit as that of the previous simulation are extracted using a Latin hypercube design. A Latin hypercube design is suitable for a random sample test because of its ability to evenly distribute random samples in the parameter domain. In the present study, 10 sample data are selected randomly for each shape. The random sample data as well as the simulation results (the curvature radii in the longitudinal direction) are presented in Tables 8 and 9. Figure 14a, b shows the graphs of the observed curvature versus the predicted curvature, and Fig. 15a, b shows the difference between the original and estimated data. As in the previous section, the percentage errors are calculated. The maximum and minimum percentage errors for the random saddle case are respectively 13.0111 and 0.1990%, while the corresponding values for the random convex case are respectively 15.2905 and 0.8198%. The mean percentage errors for the two cases are 5.7964 and 7.2577%, respectively. Overall, the errors are similar to those of the training sample data. This means that the estimations of the model fit the random sample data quite well. In other words, it is possible to use the regression model to predict the results of an FRRF process.

The prediction interval of the regression model is also calculated to enable proper prediction. A prediction interval is the

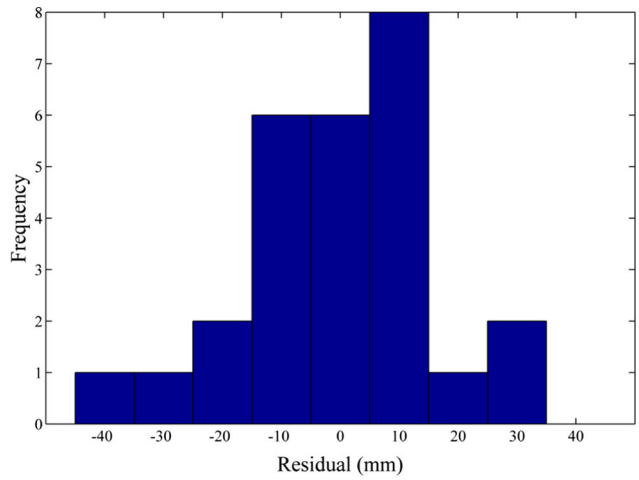

(a) Saddle shape

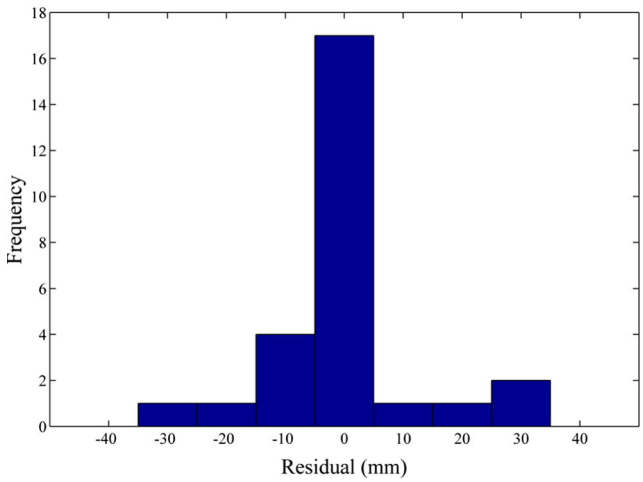

(b) Convex shape

Fig. 13 Histogram about frequency distribution

Table 8 Statistical table for saddle shape in random sample test

Number of case	Compression ratio X_1	Curvature radius of blank X_2 (mm)	Width of blank X_3 (mm)	Result (mm)
1	5.3862	532.6719	125.5861	232.80
2	9.2584	618.9142	121.3191	153.08
3	6.0976	573.2571	110.2278	228.09
4	5.6156	957.1309	119.0041	320.09
5	6.9804	839.6199	132.3784	231.49
6	8.4524	687.2206	102.2678	185.85
7	9.7514	724.5955	149.1757	163.80
8	7.6532	908.5602	144.3745	227.29
9	8.8882	771.0955	136.8794	171.37
10	7.2035	892.2177	107.5241	234.92

Table 9 Statistical table for convex shape in random sample test

Number of case	Compression ratio X_1	Curvature radius of blank X_2 (mm)	Width of blank X_3 (mm)	Result (mm)
1	0.1634	691.8053	118.4494	152.72
2	0.1458	872.7915	130.8360	120.38
3	0.1363	998.8324	123.2790	106.05
4	0.1792	626.3874	149.3364	199.03
5	0.1205	569.8017	127.3827	73.32
6	0.1311	817.5872	141.6506	99.48
7	0.1030	901.0522	113.6458	53.99
8	0.1929	735.5269	108.0822	201.14
9	0.1135	794.8920	103.6930	62.90
10	0.1070	507.1187	136.9212	60.97

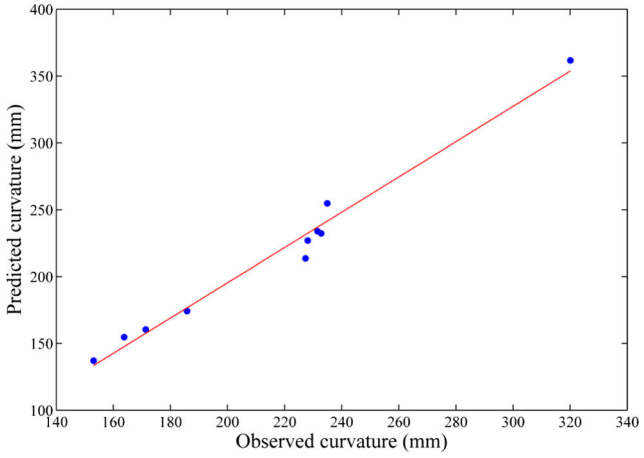

(a) Saddle shape

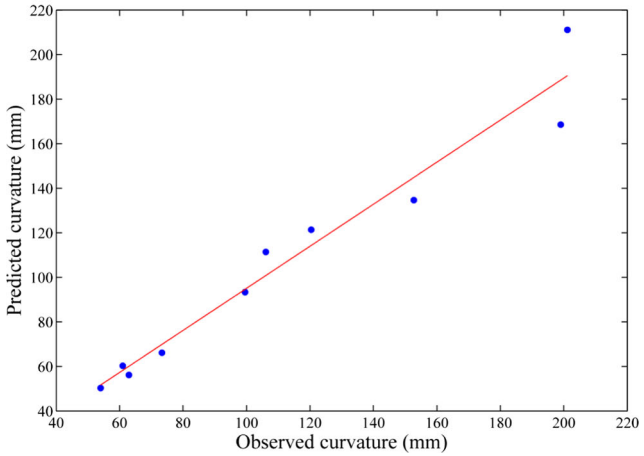

(b) Convex shape

Fig. 14 Graph of observed versus predicted curvature

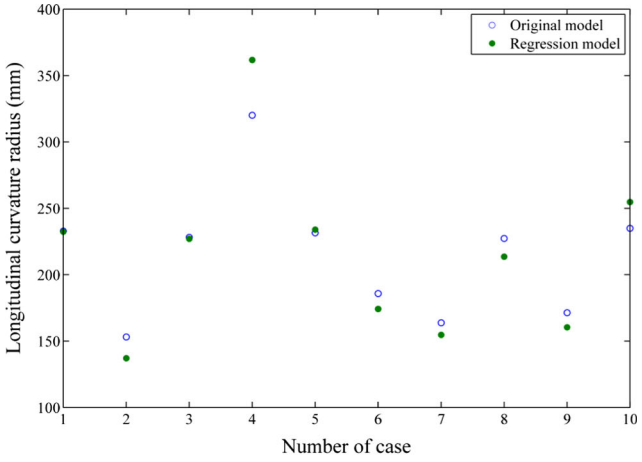

(a) Saddle shape

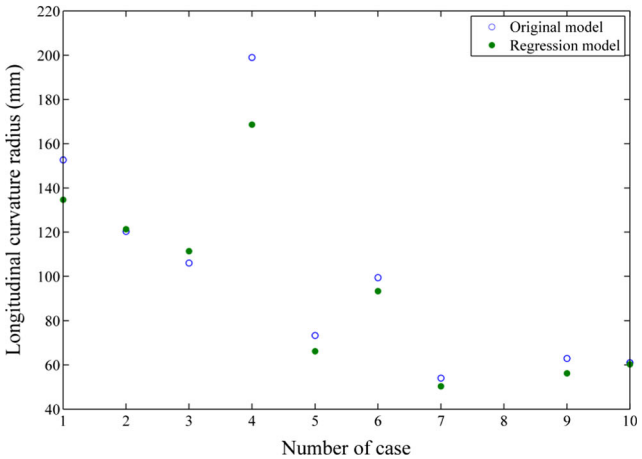

(b) Convex shape

Fig. 15 Difference between original and estimated data of random sample data

interval within which a yet-to-be-observed response is predicted to fall with a specified probability. The prediction interval is determined using Eq. 7.

$$\hat{y}(\mathbf{x}_0) - t_{\alpha/2,n-p}\sqrt{\hat{\sigma}^2\left(1+\mathbf{x}_0'\left(\mathbf{X}'\mathbf{X}\right)\mathbf{x}_0\right)} \le y_0 \le \hat{y}(\mathbf{x}_0) + t_{\alpha/2,n-p}\sqrt{\hat{\sigma}^2\left(1+\mathbf{x}_0'\left(\mathbf{X}'\mathbf{X}\right)\mathbf{x}_0\right)} \quad (7)$$

where $\mathbf{x}_0 = [1 \;\; x_{01} \;\; \cdots \;\; x_{0p}]$ and $\hat{y}(\mathbf{x}_0) = \mathbf{x}_0'\mathbf{b}$; $\hat{\sigma}^2$ can be calculated as the sum of the residual values, and $t_{\alpha/2,n-p}$ can be determined using a t statistic table and the confidence level. A confidence level of 95% is used in the present study, based on which the value of $t_{\alpha/2,n-p}$ is determined to be 2.052 from a t statistic table. The prediction interval is calculated using 10,000 samples generated by a Latin hypercube design. The results are summarised in Table 10. The mean prediction intervals for the saddle and convex cases are determined to be 45.4088 and 34.6544, respectively. The average residual of the regression model for a given case is confirmed to be less than the corresponding mean prediction interval.

5 Pre-FRRF equipment

To further verify the reliability of the above simulation results, an experimental investigation is necessary. Unfortunately, the development of the FRRF equipment is still ongoing, and this makes an actual experimental investigation impossible at the moment. However, a pre-FRRF equipment is used for the practical feasibility verification of the FRRF process in this study.

The employed pre-FRRF equipment utilises a fixed roller support, which is capable of producing only one curvature.

Table 10 Summary of prediction interval

	Saddle shape	Convex shape
Maximum prediction interval size	49.3814	37.7320
Minimum prediction interval size	44.0304	33.6651
Mean prediction interval size	45.4088	34.6544

The configuration and geometric specifications of the equipment are shown in Fig. 16. The compression ratio (tip-to-centre) used for the experiment are 7.5/2.5 and 2.5/7.5, while the curvature radius and width of the blank are 1000 and 100 mm, respectively. The blank material is Al2024-T3, which is the same as that used for the simulations. The curvature comparison is done by numerical simulation on ABAQUS using the experimental conditions. Figure 17 shows the experimental and simulation results for each shape, from which very good agreement is visually apparent. It is, however, necessary to measure the actual curvatures for precise comparison of the experimental and simulation curvatures for each case. For this purpose, the longitudinal curvature profiles along the centre lines are extracted from both results, with a 3D scanner employed for the experimental curvatures. The extracted profiles for the convex-type and saddle-type curvatures are shown in Fig. 18. As can be seen from Fig. 18a, the centre-line profiles (A-A′) for the convex-type curvature do not coincide perfectly, with the simulation producing a larger curvature radius compared to the experiment. However, the overall profiles are similar. In the case of the saddle-type curvature in Fig. 18b, the centre-line profiles (B-B′) for the simulation and experiment are almost the same.

The observed discrepancies between the simulation and experimental results are within acceptable limits, and while there is clearly room for improvement of the employed pre-FRRF equipment, the experimental results further verify the reliability of the developed regression model for predicting the curvature radius for FRRF.

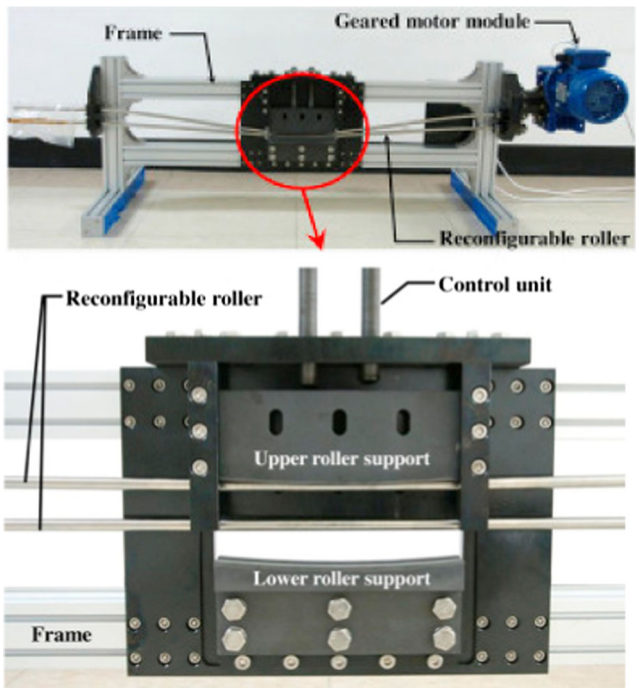

Fig. 16 Configuration of pre-FRRF equipment

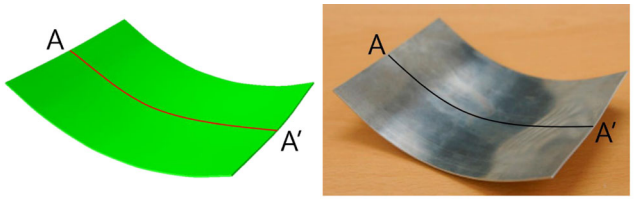

(a) Convex shape

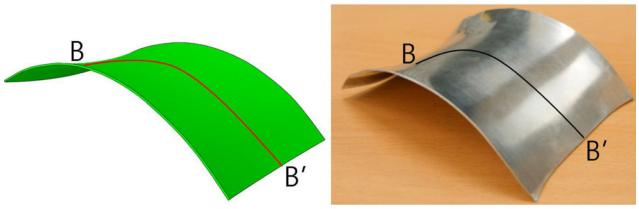

(b) Saddle shape

Fig. 17 Shape comparison for simulation with experiment

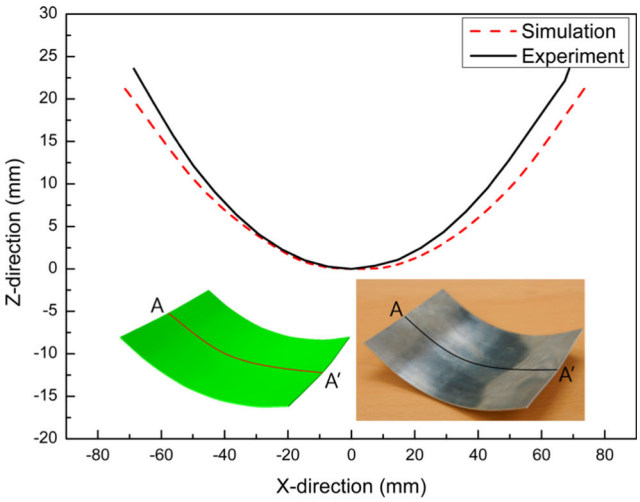

(a) Convex shape

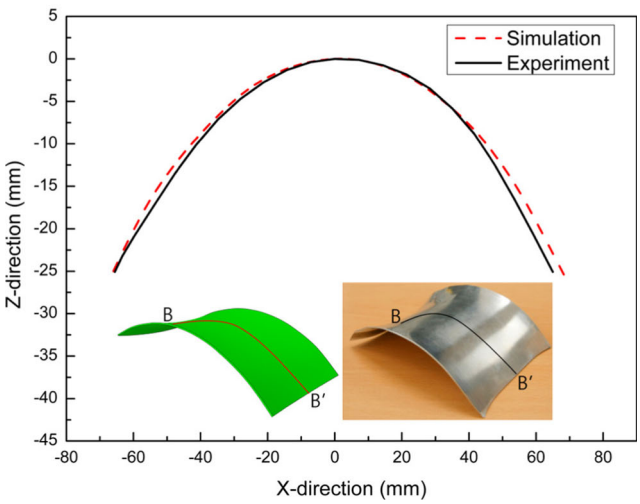

(b) Saddle shape

Fig. 18 Centre line profile of simulation and experiment

6 Conclusions

FRRF is investigated in this study to determine the effects of the input parameters on the forming results in the longitudinal direction. The response surface methodology is used to develop a model for predicting the longitudinal curvature of a sheet metal shaped by the FRRF process. The forming process is numerically simulated to obtain sample data for regression analysis. The simulation results verify the feasibility of forming saddle and convex surfaces by FRRF, and the regression analysis of sample simulation data is used to develop a model for predicting the forming results. The polynomial regression model is then used to derive an appropriate estimation equation. To validate the regression analysis, a goodness-of-fit test is conducted and the R-squared values, NRMSE values, and residual data are examined. The test results reveal good fit of the simulation data and thus validate the regression model. To further verify the simulation results, experiments are conducted using pre-FRRF equipment. Good agreement is observed between the experimental and simulation results, although this only basically verifies the reliability of the sample data. The results of this study confirm the feasibility of statistically predicting the curvature produced by an FRRF process. Further study is planned for additional experimental verification of the prediction model using the actual FRRF equipment.

Acknowledgements This work was supported by the National Research Foundation of Korea (NRF) grant funded by the Korea government (MSIP) through the Engineering Research Centre (No. 2012R1A5A1048294) and the Human Resource Training Program for Regional Innovation and Creativity through the Ministry of Education and the National Research Foundation of Korea (NRF-2015H1C1A1035499).

References

1. Heo SC, Seo YH, Song WJ, Kim J, Kang BS, Ku TW (2008) Numerical and experimental investigation on product configuration using flexible forming process. Steel Res Int 79(1):640–647
2. Quan GZ, Ku TW, Kang BS (2011) Improvement of formability for multi-point bending process of AZ31B sheet material using elastic cushion. J Precis Eng Manuf 12(6):1023–1030
3. Wang D, Li MZ, Cai ZY (2014) Investigation on forming precision of flexible rolling process for three-dimensional surface parts of different sheet materials. Procedia Eng 81:227–232
4. Yoon JS, Son SE, Song WJ, Kim J, Kang BS (2014) Study on flexibly-reconfigurable roll forming process for multi-curved surface of sheet metal. Int J Precis Eng Manuf 15(6):1069–1074
5. Myers RH, Montgomery DC, Anderson-cook CM (2009) Response surface methodology—process and product optimization using designed experiments, 3rd edn. Wiley, New Jersey, pp 13–62
6. Ganjigatti JP, Pratihar DK, Roy Choudhury A (2007) Global versus cluster-wise regression analyses for prediction of bead geometry in MIG welding process. J Mater Process Technol 189:352–366
7. Çaydaş U, Hasçalık A (2008) A study on surface roughness in abrasive waterjet machining process using artificial neural networks and regression analysis method. J Mater Process Technol 202:574–582
8. Kamal Bashah NA, Muhamad N, Deros BM, Zakaria A, Ashari S, Mobin A, Mohd Abdul Lazat MS (2013) Multi-regression modelling for springback effect on automotive body in white stamped parts. Mater Des 46:175–190
9. Seo YH, Kang BS, Kim J (2012) Study on relationship between design parameters and formability in flexible stretch forming process. Int J Precis Eng Manuf 13(10):1797–1804
10. Kang BS, Yoon JS (2013) Sheet forming apparatus with flexible rollers. PCT patent (PCT2013134KR)